Research on a Synchronous Reluctance Drive System

MING-TSAN LIN AND TIAN-HUA LIU

Department of Electrical Engineering
National Taiwan Institute of Technology
Taipei, Taiwan, R.O.C.

ABSTRACT

This paper presents research on a synchronous reluctance drive system First, the modeling of a synchronous reluctance motor is studied. In addition, the procedures for measuring the parameters of the synchronous reluctance motor are described. Then, under field-oriented control, a simplified model of the whole closed-loop drive system is proposed. Based on the simplified model, a sliding mode with a fuzzy controller is designed. Using this new controller, the system has fast response and good disturbance rejection capability. Next, the implementation of the whole system is described. This includes: three software programs, a high performance 32-bit C30 digital signal processor system, and some simple hardware circuits. Finally, some experimental and simulated results are shown. The experimental waveforms validate the simulated results. This paper proposes a systematic design for a synchronous reluctance drive.

Key Words: synchronous reluctance motor, sliding mode control, digital signal processor

I. Introduction

Compared with the induction drive or the permanent magnet synchronous drive, the synchronous reluctance motor (SRM) has many advantages, for example, simple and rugged construction, high efficiency due to the absence of a rotor winding, and low cost. In the past, the SRM was only used in variable frequency applications with open-loop control, such as fiber spinning and pumps. Recently, tremendous progress has been made in electrical machine design and power electronics. Many researchers have studied using the SRM as a servo drive. The closed-loop control of a SRM with position and current sensors has been examined by many authors. For example, Xu *et al.* (1991) studied vector control of an SRM including saturation and iron loss, and Betz (1991) proposed a control method of SRM. Chiba and Fukao (1992) developed a DSP based high performance SRM drive system. Xiang and Nasar (1995) presented a fully digital control strategy for an SRM drive. However, only the proportional-integral (PI) controller was used as a speed-loop or a position-loop in those systems. Moreover, the parameters of the PI controller were obtained by trial and error. In this paper, a systematic controller design for the SRM drive system is proposed. First, the mathematical model and the measuring procedures for the parameters of the motor will be presented. Then, a simplified model of the system based on vector control will be proposed. Based on the simplified model, the design of a sliding mode with a fuzzy controller will be described. Finally, some simulated and experimental results will be shown. The results not only validate the theoretical analysis, but also show that this new control method performs better than does the traditional PI controller.

II. Mathematical Model and Parameters Determination

The structure of the SRM is shown in Fig. 1. The motor has three parts: a stator, a rotor, and an air gap. The stator has uniform distributing windings. The rotor, however, has no exciting winding to produce electromagnetic torque. It only has damping winding to start the motor. When the motor is operated in steady-state, the damping winding has no function. The torque is, therefore, produced by the reluctance difference of the d-axis and q-axis. The air gap of the motor is not uniform in order to produce larger reluctance torque.

Although the structure of the SRM is very simple, its mathematical model, which was proposed by Liu and Lin (1994), is very complex. The mathematical model of a three-phase, Y-connected, SRM with damping winding can be described in the a-b-c stationary frame. However, to ease the controller design task, the
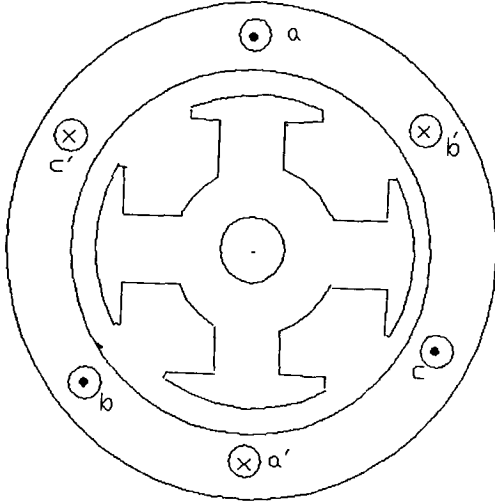
Fig. 1. The structure of the SRM.

SRM dynamic equations are usually expressed in a d-q synchronous rotating reference frame. In the d-q synchronous frame, the dynamic equations are

$$pi_{ds}=[(V_{ds}-r_si_{ds}+\omega_r(L_{qs}i_{qs}+L_{mq}i_{kq}))L_{dr}$$

$$+L_{md}r_ki_{kd}]/(L_{ds}L_{dr}-L_{md}^2) \qquad (1)$$

$$pi_{qs}=[(V_{qs}-r_si_{qs}-\omega_r(L_{ds}i_{ds}+L_{md}i_{kd}))L_{qr}$$

$$+L_{mq}r_ki_{kq}]/(L_{qs}L_{qr}-L_{mq}^2) \qquad (2)$$

$$pi_{kd}=[(V_{ds}-r_si_{ds}-\omega_r(L_{qs}i_{qs}+L_{mq}i_{kq}))L_{md}$$

$$-L_{ds}r_ki_{kd}]/(L_{ds}L_{dr}-L_{md}^2) \qquad (3)$$

$$pi_{kq}=[(V_{qs}-r_si_{qs}+\omega_r(L_{ds}i_{ds}+L_{md}i_{kd}))L_{mq}$$

$$-L_{qs}r_ki_{kq}]/(L_{qs}L_{qr}-L_{mq}^2), \qquad (4)$$

where p is the differential operator d/dt, i_{ds} and i_{qs} are the d-q axis stator currents, i_{kd} and i_{kq} are the d-q axis rotor currents, V_{ds} and V_{qs} are the d-q axis stator voltages, r_s is the stator resistance, ω_r is the electrical speed, L_{ds} and L_{qs} are the d-q stator inductances, L_{md} and L_{mq} are the d-q axis magnetizing inductors, L_{dr} and L_{qr} are the d-q axis rotor inductances, and r_k is the rotor resistance. The electro-mechanical equation of the motor is

$$p\omega_r=\frac{1}{J_m}(T_e-T_l-B_m\omega_r), \qquad (5)$$

where J_m is the inertia constant, T_l is the load torque, B_m is the viscous frictional coefficient, and the motor

torque can be expressed as

$$T_e=\frac{3}{2}(\frac{P}{2})(L_{ds}-L_{qs})i_{ds}i_{qs}, \qquad (6)$$

where P is the number of the poles of the motor.

1. Parameters Determination

A. L_{ds}, L_{qs}, and r_s

Let $p=j\omega$, and substitute $p=j\omega$ into Eqs. (1)-(4). We can thus derive the real and reactive powers as

$$P=-V^2\frac{r_s-0.5(X_d-X_q)\sin2\delta}{r_s^2+X_dX_q} \qquad (7)$$

$$Q=V^2\frac{\cos^2\delta X_q+\sin^2\delta X_d}{r_s+X_dX_q}, \qquad (8)$$

where V is the phase voltage, δ is the load angle of the motor, P is the real power, and Q is the reactive power. In this study, we used a simple method to measure L_{ds}, L_{qs}, and r_s. This method has been presented in previous papers. Using this method, the three parameters can be easily obtained without special equipment. The curve of the real power to reactive power is derived from Eqs. (7) and (8) and is shown as Fig. 2. The testing procedures are based on the fact that the operating points of the SRM in the PQ plane lie in a circle occupying the first and fourth quadrants. According to this figure, we can compute P_{max}, P_{min}, and Q_{min} from the measurement data. Then, we can calculate r_s, L_{ds}, and L_{qs}. The parameter measuring steps of this procedure are as

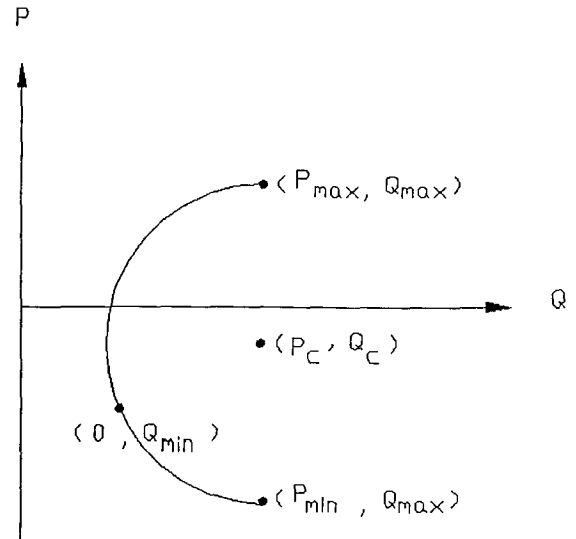

Fig. 2. The curve of the real power to reactive power

follows:

Step 1: Mount the dynamometer on the motor.

Step 2: Connect instruments and a three-phase AC source to the motor.

Step 3: Measure the related data, voltages, currents, speed, torque, and real and reactive powers, while the load of the dynamometer is controlled to obtain different loads.

Step 4: Repeat step 3 until enough data is obtained.

Step 5: Select three significant cases of step 4, and use the data to calculate the center point (P_c, Q_c) and the radius R of the circle as shown in Fig. 2.

Step 6: The center and the radius R are computed according to the following equation:

$$\begin{bmatrix} Q_c \\ P_c \\ P_c^2 + Q_c^2 - R^2 \end{bmatrix} = \begin{bmatrix} -2Q_1 & -2P_1 & 1 \\ -2Q_2 & -2P_2 & 1 \\ -2Q_3 & -2P_3 & 1 \end{bmatrix}^{-1} \begin{bmatrix} -S_1^2 \\ -S_2^2 \\ -S_3^2 \end{bmatrix}, \qquad (9)$$

where Q_1, Q_2, and Q_3 are the measured reactive powers of the three cases; P_1, P_2, and P_3 are the measured real powers of the three cases; and S_1, S_2, and S_3 are the measured apparent powers of the three cases. From Fig. 2, the maximum real power, minimum real power, and minimum reactive power are described as

$$P_{max} = P_c + R \qquad (10)$$

$$P_{min} = P_c - R \qquad (11)$$

$$Q_{min} = Q_c - R. \qquad (12)$$

Then, the machine parameters are calculated by using the following equations:

$$\frac{r_s}{\omega_r L_{qs}} = \frac{1}{2} \frac{|P_{min}| - |P_{max}|}{|Q_{min}|} \qquad (13)$$

$$\frac{L_{ds}}{L_{qs}} = 1 + \frac{|P_{max}| + |P_{min}|}{|Q_{min}|} \qquad (14)$$

and

$$\omega_r L_{ds} = \frac{V^2}{[(r_s/(\omega_r L_{qs}))^2(L_{qs}/L_{ds}) + 1]|Q_{min}|}. \qquad (15)$$

Substitute the data from the above mentioned three cases into Eqs. (9)-(15). We can obtain the parameters L_{ds}, L_{qs}, and r_s:

B. L_{md}, L_{mq}, L_{kd}, L_{kq}, r_k

Generally speaking, the leakage inductance is

almost equal to 10% of the self-inductance. The mutual inductance, therefore, is almost equal to 90% of the self-inductance. In addition, we can assume that the leakage inductance of the rotor equals that of the stator. The resistance of the rotor is measured by using the block-rotor test. The parameters L_{md}, L_{mq}, L_{kd}, L_{kq}, and r_s, thus, are obtained:

C. J_m and B_m

The inertia of the motor, J_m, is calculated according to the geometric structure of the rotor. The inertia of the dynamometer, J_l, is obtained from its geometric structure also. In the proposed system, the total inertia, J_t, is equal to the summation of J_m and J_l because the dynamometer is directly coupled to the motor. The total viscous coefficient of the system can be obtained easily. First, we couple the dynamometer and the motor. Then, we set the external load, T_l, to zero and measure the torque, T_e, to speed ratio while the motor is operated at different speeds. The total viscous coefficient, B_t, is equal to the ratio of T_e/ω_{rm}.

2. Simplified Model of the Drive System

The three phase real currents i_a, i_b, and i_c are forced to follow the three current commands. Therefore, we assume that $i_a^* \cong i_a$, $i_b^* \cong i_b$, and $i_c^* \cong i_c$. The torque equation, which is shown as Eq. (6), can be expressed as

$$T_e \cong \frac{3}{2} \left(\frac{P}{2}\right)(L_{ds} - L_{qs}) i_{ds}^* i_{qs}^*. \qquad (16)$$

Figure 3 shows the block diagram of the simplified model of the closed-loop drive system. First, the speed controller determines the current commands, i_{ds}^* and i_{qs}^*, according to the speed error and speed-loop control algorithm. Then, the torque of the motor is produced. Finally, the speed is fed back, and a closed-loop system is, thus, achieved. The original mathematical model is a high-order, nonlinear, coupled system. It is very difficult to design a controller. However, after suitably simplifying the mathematical model, a speed-loop controller can be easily designed. In Eq. (16), the
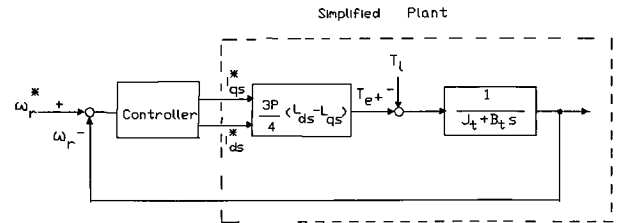

Fig. 3. Block diagram of the simplified system.

torque is proportional to the product of i_{ds}^* and i_{qs}^*. If we select i_{ds}^* as a constant, the torque is proportional to i_{qs}^*. This is called "field-oriented control." On the other hand, if we choose $i_{ds}^* = i_{qs}^*$, the torque/current is maintained as a maximum value. This is, thus, called "maximum torque control." In this case, the torque is maximum for a fixed stator current; however, it is very difficult to design a speed-loop controller because the torque is proportional to i_{ds}^{*2} or i_{qs}^{*2}.

III. Controller Design

1. Sliding Mode Controller

A sliding mode control system is insensitive to the parameter variation and load disturbance effects of a plant. The response of this system is related to the sliding line. However, it is not related to the parameters of the plant or the external load. The sliding mode controller has been used as a position-loop controller for a servo drive because the position signals and the speed signal are easy to detect. The sliding mode control is difficult to use as a speed-loop controller because the acceleration, the derivative of speed, is not easy to measure. In this paper, a sliding mode controller with an acceleration estimator is proposed. First, we choose $x_1(t)$ as the speed error $\Delta\omega_r$ and $x_2(t)$ as $-\dot{\omega}_r$. Then, the dynamic equation of the plant is

$$\begin{bmatrix} \dot{x}_1(t) \\ \dot{x}_2(t) \end{bmatrix} = \begin{bmatrix} 0 & 1 \\ 0 & -B_t/J_t \end{bmatrix} \begin{bmatrix} x_1(t) \\ x_2(t) \end{bmatrix} + \begin{bmatrix} 0 \\ -K_t/J_t \end{bmatrix} i_q(t) \qquad (17)$$

$$y(t) = \begin{bmatrix} 0 & -1 \end{bmatrix} \begin{bmatrix} x_1(t) \\ x_2(t) \end{bmatrix}, \qquad (18)$$

where $x_1(t)$ and $x_2(t)$ are states, $y(t)$ is the output, B_t is the friction coefficient of the motor and load, J_t is the inertia of the motor and load, and K_t is the torque constant of the motor. In order to reduce the high frequency vibration of the speed, we have to smooth the controller output signal $u(t)$. Therefore, an integration controller is inserted into the output of the sliding mode controller. The relationship between the output of the sliding mode controller $u(t)$ and the q-axis current $i_q(t)$ can be expressed as

$$i_q(t) = \int u(t)\, dt. \qquad (19)$$

The sliding line σ can be chosen as

$$\sigma = Cx_1(t) + x_2(t) = 0, \qquad (20)$$

where C is a constant which is chosen by a designer. Let $u(t) = \psi x_1(t)$, where ψ is a variable scaler. When σx_1 is greater than or equal to zero, ψ is set as α; however, when σx_1 is less than zero, ψ is changed to β. The condition for the existence of the sliding regime is $\lim \sigma \dot{\sigma} \le 0$. Then, by substituting Eqs. (17)-(20) into the condition, we can obtain the controller parameters, α and β, to satisfy the following inequality:

$$\beta \le J_t \, C[(B_t/J_t) - C] \le \alpha. \qquad (21)$$

If we obtain the acceleration by calculating the position difference with time, then the signal will consist of many high frequency harmonics. These harmonics of the signal can affect the servo system performance. The transfer function of the estimator is $\frac{s}{\tau_d s + 1}$. When τ_d is selected as zero, the estimator performs as a derivative. However, when τ_d is increased, the steady-state error of the estimator is increased. So, the choice of τ_d depends on experience.

2. Sliding Line Adjusting Method

From Eq. (20), we can easily obtain the speed response of the drive system. The response of the speed is related to the slope of the sliding line and is expressed as

$$\omega_r(t) = \omega_r^*(1 - e^{-Ct}), \qquad (22)$$

where ω_r^* is the speed command, $\omega_r(t)$ is the speed response, and C is the slope of the sliding line. If C is selected as a high value, the speed response is faster; however, the chattering of the speed response is serious. On the other hand, if we select a small C, the speed response is slower. The chattering phenomenon, however, is reduced. In order to obtain both faster response and a small chattering phenomenon in steady-state, the slope C has to be adjusted automatically. The slope of the sliding line is

$$C(t_2) = C(t_1) + \int_{t_1}^{t_2} \kappa(\lambda)\, d\lambda, \qquad (23)$$

where C is the slope of the sliding line, and $\kappa(\lambda)$ is the adjusting factor.

3. Fuzzy Control Law

In order to adjust the slope of the sliding line, a fuzzy control law is proposed here. The fuzzy control
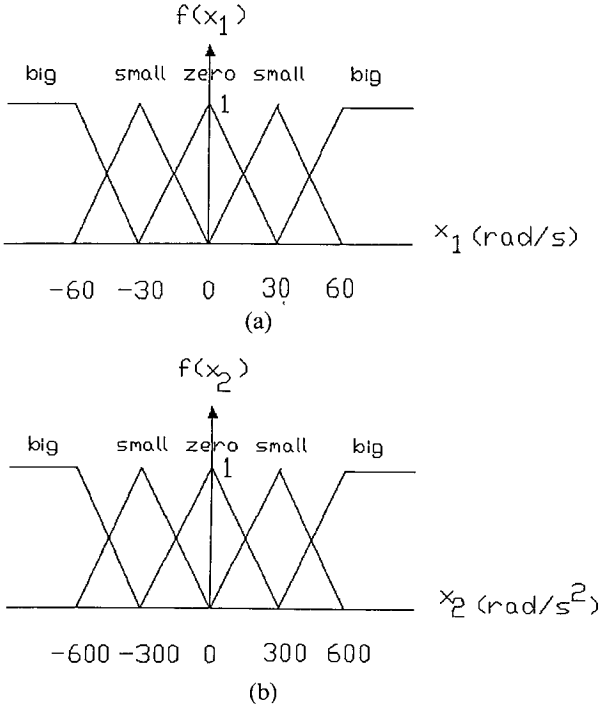
f(x₁)

f(x₂)

Fig. 4. Membership functions (a) x_1 state (b) x_2 state.

law is used to adjust the slope of the sliding line. The fuzzy control algorithm consists of the following three steps:

A. Fuzzification

Figure 4 shows the membership functions for the states of x_1 and x_2. From Fig. 4, we can understand that the difference of state x_1 from big to small, and small to zero is 30 rad/sec, and the difference of state x_2 is 300 rad/sec². The shapes of the membership functions are triangular in this paper.

B. Fuzzy-Reasoning Control Law

There are seven control laws for fuzzy-reasoning. They are as follows:

IF $|x_1|$ is big, THEN ζ is positive big;
IF $|x_1|$ is small and $|x_2|$ is big, THEN ζ is negative small;
IF $|x_1|$ is small and $|x_2|$ is small, THEN ζ is zero;
IF $|x_1|$ is small and $|x_2|$ is zero, THEN ζ is positive small;
IF $|x_1|$ is zero and $|x_2|$ is big, THEN ζ is negative big;
IF $|x_1|$ is zero and $|x_2|$ is small, THEN ζ is negative small;
IF $|x_1|$ is zero and $|x_2|$ is zero, THEN ζ is zero;
where ζ is the output of the fuzzy-reasoning control. When ζ is big, its value is set as 1; when ζ is small,

its value is equal to 0.5; when ζ is zero, its value is set as 0.

C. Defuzzification

The intersection of the grade of the membership functions x_1 and x_2, which considers both the effects of the two states x_1 and x_2, is

$$\mu_n = \min(\mu(x_1),\ \mu(x_2)), \qquad (24)$$

where μ_n is the grade of the membership function in the different categories. Then, we use the center of area (COA) method to obtain the final value of the adjusting factor κ through properly scaling coefficient, λ:

$$\kappa = (\sum_{n=1}^{n=m} \mu_n \zeta \lambda)/(\sum_{n=1}^{n=m} \mu_n), \qquad (25)$$

where m is the total number of different categories of the membership functions, λ is the scaling coefficient.

IV. Implementation

The implemented system consists of two major parts: hardware and software. The current-loop and speed-loop controllers are executed by a DSP, TMS320C30. The DSP executes the current-loop control law in 50 μs, and the speed-loop control law in 1 ms. The whole drive system, therefore, is a multiple sampling rate system.

1. Hardware System

The hardware consists of four parts: an inverter, a driver, a current sensing circuit, and a position and speed detecting circuit. The inverter is constructed using insulated-gate bipolar transistors (IGBTs). When the IGBTs are switched, many spike voltages are produced between the collectors and emitters of the IGBTs. Snubber circuits, therefore, are used to reduce the spike voltages. The parameters of the snubber circuits are: R_s=80 Ω, C_s=0.1 μf. High speed diodes are used to control the direction of energy flow. The IGBTs are Fuji 2MBI50-120.

The driving circuit is shown in Fig. 5(a). The circuit is based on the integrated circuit Fuji EXB840. This circuit has many advantages: simple construction, isolated input and output signals, and the over current protection function. The principle of the circuit is simple. When the control signal is high, the photo-transistor is turned on. Then, there is a 15V voltage across G_1 and E_1, and the IGBT,

(a)

(b)

To DSP (Speed Signal)

To DSP Control Signal
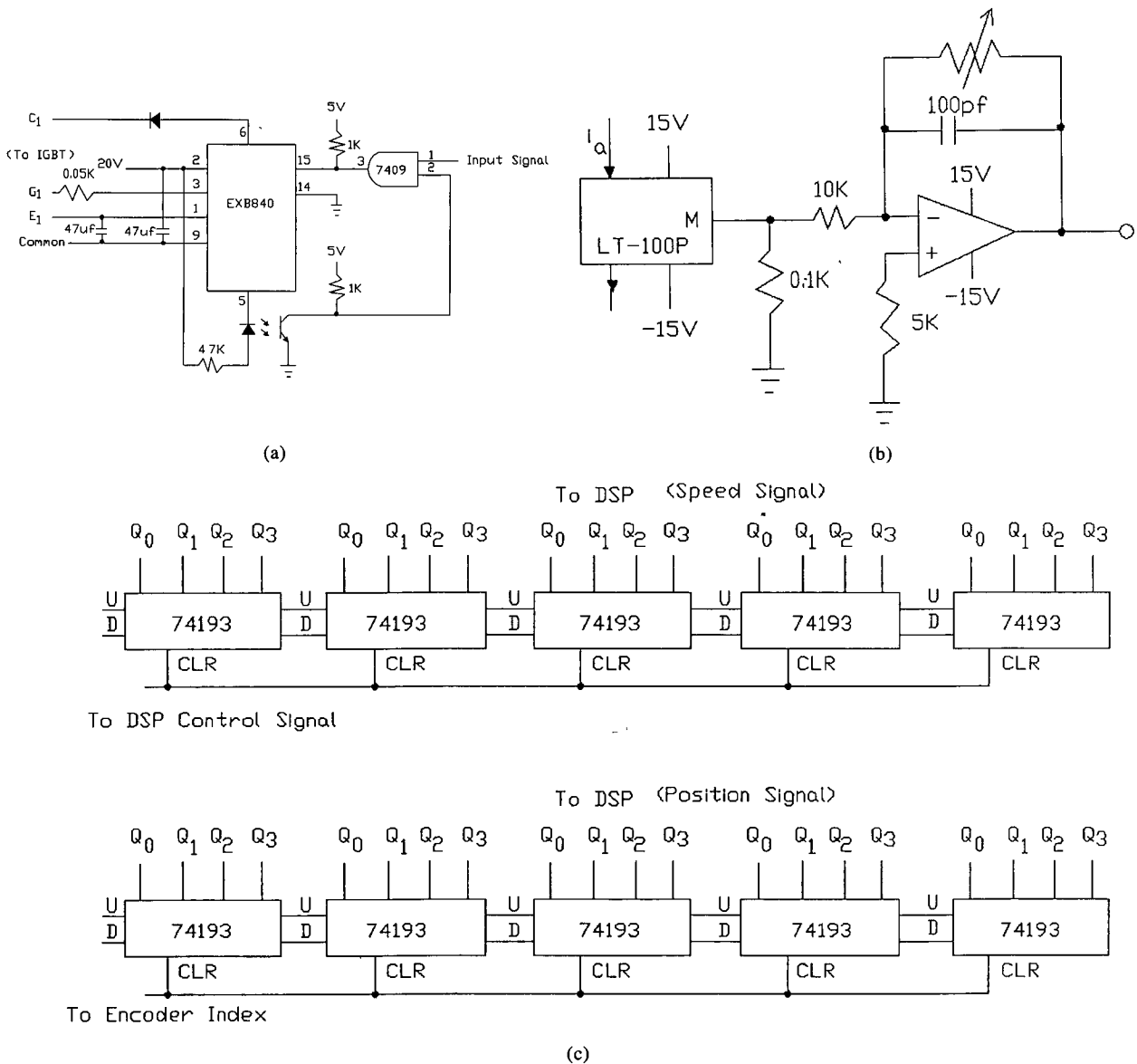
To DSP (Position Signal)

To Encoder Index

(c)

Fig. 5. The hardware circuits. (a) Driver. (b) Current sensing circuit. (c) Position and speed detecting circuit.

therefore, is turned on. On the other hand, when the control signal is low, the photo-transistor is turned off. There is a -5 V voltage across G_1 and E_1, and the IGBT can be turned off after a short period of time. In addition, when the current of the IGBT exceeds the limit, the circuit quickly cuts off drive signals to turn off the IGBTs. The current sensing circuit is shown in Fig. 5(b). The major element is a Hall-effect sensor. The ratio of the primary current/second current is 1000:1. The maximum current limitation of the sensor is 100 A, and its frequency bandwidth is 30 KHz. By suitably adjusting the variable resistor, we can obtain a 0.5 V output voltage when an 1 A current flows through the primary side

of the current sensor. A 100 pf capacitor is used as a low pass filter to reduce the noise of the current signals. The motor position and speed detecting circuit is shown in Fig. 5(c). First, the circuit multiplies the pulses by 4. Using this method, an 8000 pulses/revolution output signal can be produced. The resolution of the whole system, therefore, is improved. A direction decision signal, which can determine the rotating direction of the motor, is sent to a D-type flip/flop. Then, it controls the increase or decrease of pulses. Four cascade TTL 74193 up/down counters are used to convert the series pulses into parallel sequence pulses. The upper circuit is used as the position counter of the motor. The lower circuit is used as the speed
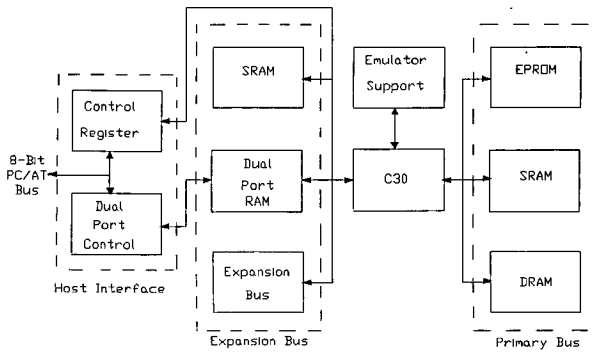
Fig. 6. The configuration of the C30 DSP System.

counter of the motor. The position signal is sensed every 50 μs. The speed signal, however, is detected every 1 ms.

2. Software Program

The software was developed in a DSP system. The DSP system is a product of the Texas Instruments Company. The block diagram of the system is shown in Fig. 6. The DSP system consists of two major boards: an emulator board and an application board. The emulator board is used as an interface device between the DSP and the personal computer. In addition, it also supports many functions for the application board. The application board consists of a DSP chip and two dual ports to communicate with peripheral devices. The system is, therefore, flexible enough so that RAM, ROM, I/O port, and other peripheral devices can be connected.

The software has three major programs: a main program, a speed-loop interrupt service routine, and a current-loop service routine. These programs were designed using DSP instructions directly, not using any high level language. Using this method, the execution time of the DSP system is very short, and we can obtain a high performance digital control. The processing steps of the three programs are described below. (In this paper, only the field-oriented control algorithm is shown. The maximum torque control can be easily modified according to the field-oriented control algorithm.)

A. Main Program

Step 1. Initialize the DSP system:
Step 2. Scan to determine if any message is input from the keyboard of the computer.
If the new message is acceptable, go to step 3.
If the new message is unacceptable, go to

step 4.
If no message is input, go to step 5.
Step 3. Update the speed command, parameters, or any required data.
Go to step 2.
Step 4. Display the error message.
Go to step 2.
Step 5. Go to step 2.

B. Speed-Loop Interrupt Service Routine

Step 1. Set interrupt flag as a disabled state.
Step 2. Read the speed of the motor.
Step 3. Execute the acceleration estimate subroutine.
Step 4. Compute the speed error.
Step 5. Execute the fuzzy control law to determine the slope C of the sliding line.
Step 6. Use the slope C and the measured states to compute the sliding mode control output.
Step 7. Integrate the output signal to obtain the

Table 1. The Measured Parameters of the SRM

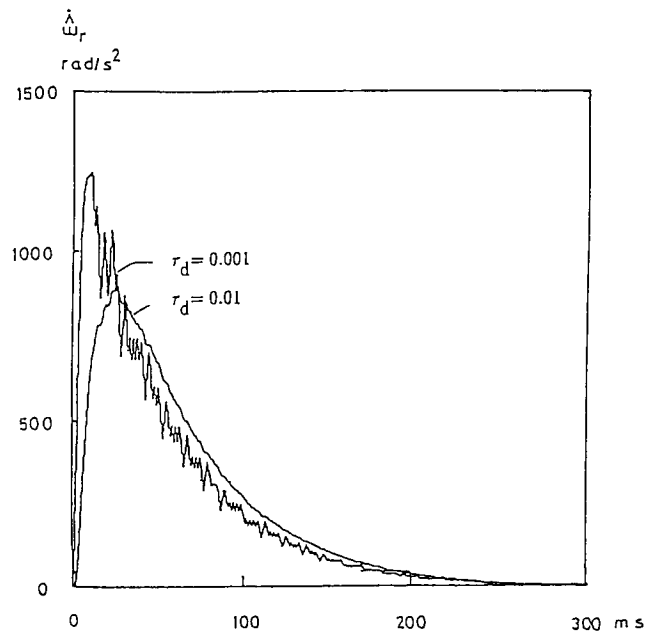| r_s	2.0Ω	r_k	0.94Ω
L_{qs}	0.0486H	L_{ds}	0.1244H
L_{md}	0.112H	L_{mq}	0.04374H
L_{dr}	0.0124H	L_{qr}	0.0124H
J_t	0.02222N.m/sec^2		
B_t	0.001N.m/sec		

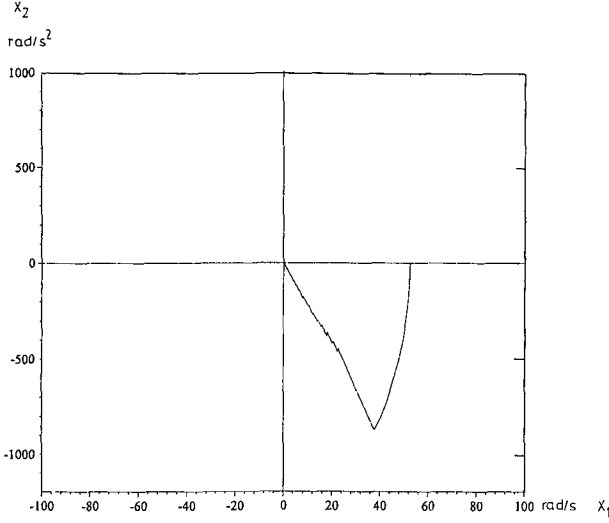Fig. 7. The effect of τ_d on the acceleration estimator.

Fig. 8. Experimental phase plane curve.

current commands, i_{qs}^*.

Step 8. Set the interrupt flag as an enabled state.

Step 9. Return to the main program.

3. Current-Loop Interrupt Service Routine

Step 1. Set the interrupt flag as a disabled state.

Step 2. Read the three phase currents i_a, i_b, and i_c.

Step 3. Read the position of the motor θ_e.

Step 4. Look up the table to obtain $\sin\theta_e$, $\sin(\theta_e - 120°)$, and $\sin(\theta_e + 120°)$.

Step 5. Multiply i_{qs}^* by $\sin\theta_e$, $\sin(\theta_e - 120°)$, and $\sin(\theta_e + 120°)$ to obtain i_a^*, i_b^*, and i_c^*.

Step 6. Compute the current derivations Δi_a, Δi_b, and Δi_c.

Step 7. Determine and output the switching pattern to the driving circuit.

Step 8. Set the interrupt flag as an enabled state.

Step 9. Return to the main program.

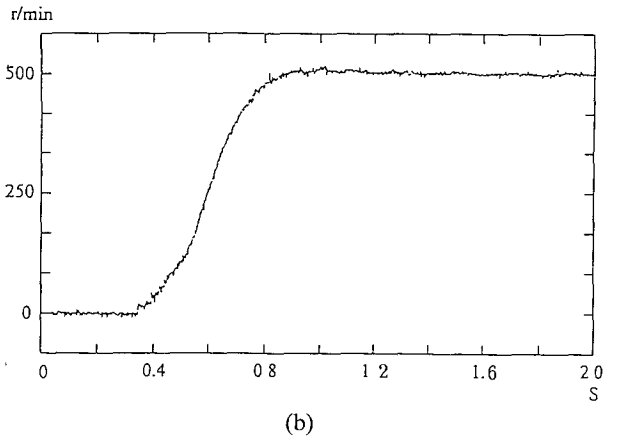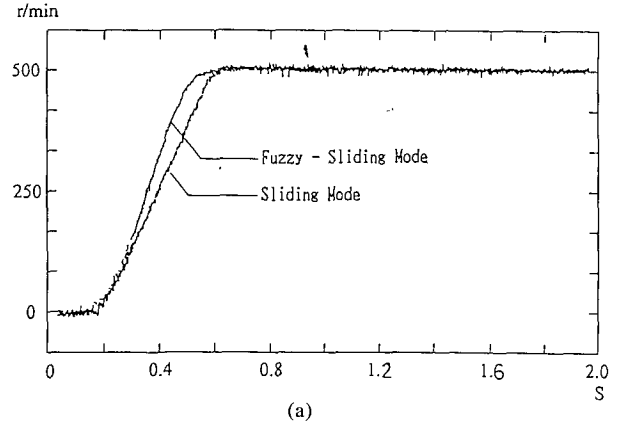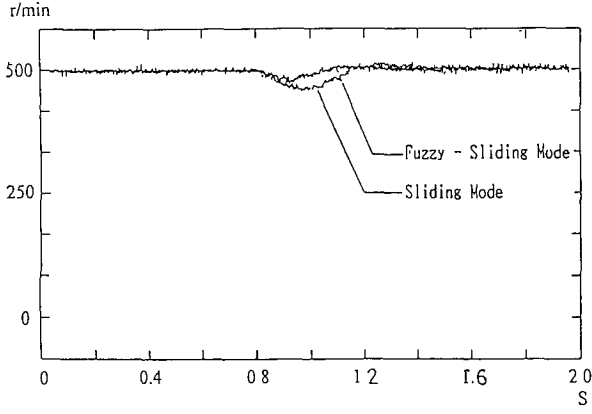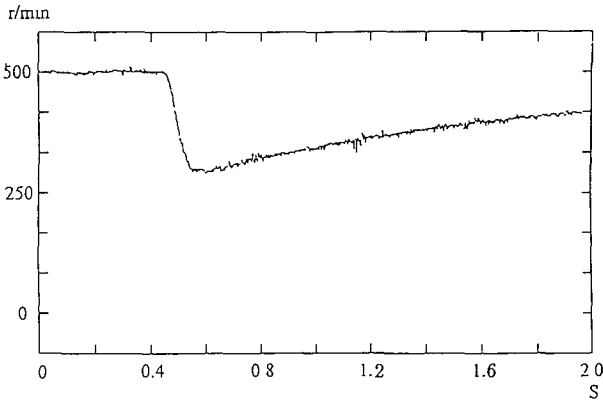Fig. 9. Measured steady-state a-phase currents.

Fig. 10. Speed responses, (a) proposed method, (b) PI controller.

V. Simulation and Experimental Results

To execute the speed-loop control algorithm, a DSP-based control system has been implemented. The DSP is TMS 320C30, with a 60 ns single cycle instruction execution time and floating-point operation. The hardware circuit consists of an inverter and some sensing circuits. The sampling interval of the system is 1 ms. The motor is 3 phase, 4 pole, 220 V, 0.75 HP, and its parameters are shown in Table 1. Some simulation and experimental results are shown here. Figure 7 shows the effect of τ_d for the acceleration estimator. If τ_d is set as a small value, the estimator is accurate but the noise increases. Figure 8 shows the experimental phase plane curve of states x_1 and x_2. Figure 9 is the steady-state a-phase currents. The fuzzy sliding mode controller performed well. Figure 10 is the speed responses of the motor, which was operated at 500 r/min. The proposed method performed better. The parameters of the PI controller were selected as $K_p = J_m C/K_t$ and $K_I = B_m C/K_t$. Using these parameters, the PI controller based system could obtain a dominant pole

Fig. 11. Load disturbance responses, (a) proposed method, (b) PI controller.

Fig. 13. The responses when the motor was reversed, (a) speed, (b) current.

similar to that of the proposed system. According the figure, the sliding mode controller has a faster response than does the PI controller. Figure 11 shows the load disturbance rejections of 2 N.m for the different controllers, and the sliding mode controller is found to perform better than the PI controller once again. The same results were obtained when the external was varied.
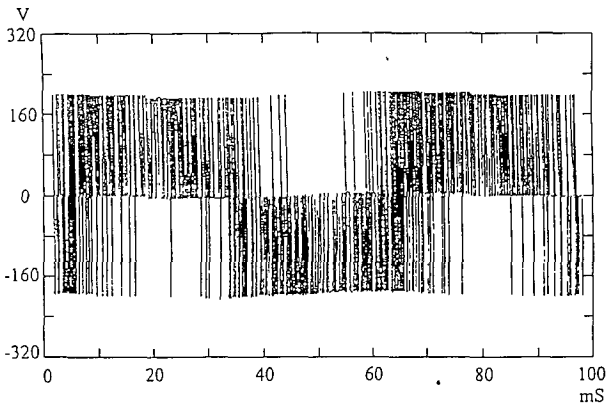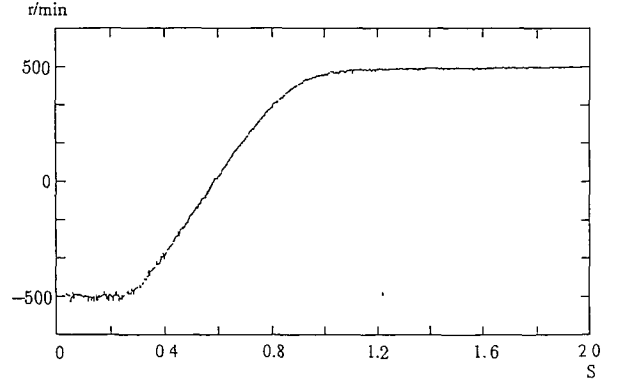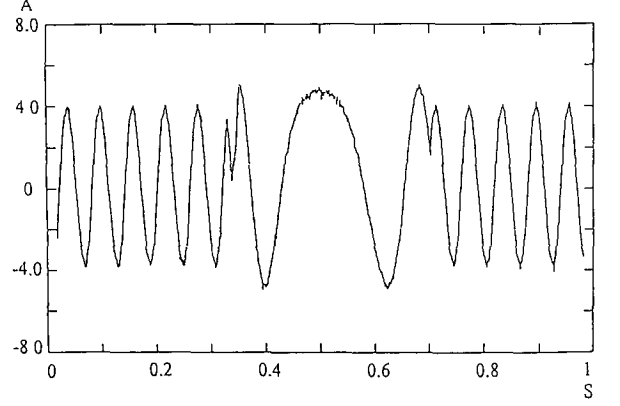

Fig. 12. Measured line-line voltage V_{ab}.

Because of space limitations, only one case is shown here. Figure 12 shows the measured voltage V_{ab}. The switching frequency is about 20 KHz. Figure 13 shows the measured responses when the motor was reversed from -500 r/min to 500 r/min. When the speed command was increased, the rise time of the system increased also. For example, when the motor was under load and its speed was reversed from -1000 r/min to 1000 r/min, the required time was about 800 ms. The reason is that there is a maximum current limitation in the drive system.

VI. Conclusions

This paper has presented the design and implementation of an SRM drive based on a sliding mode control. One of the key steps is successful implementation of the controller using a DSP. The other important contribution is that the system uses a sliding mode with a fuzzy controller. This controller performs better than a traditional PI controller. The results presented in the paper represent a first step toward the design of an SRM drive employing advanced control

techniques.

References

Betz, R. E. (1991) Control of synchronous reluctance machines. *Conf. Rec. IEEE/IAS Annu. Meet.*, pp. 456-462. Dearborn, MI, U.S.A.

Chiba, A. and T. Fukao (1992) A closed-loop operation of super high-speed reluctance motor for quick torque response. *IEEE Trans. Ind. Appl.*, **28**, 600-606.

Liu, T. H. and M. T. Lin (1994) DSP-based sliding mode control for a sensorless synchronous reluctance motor drive. *20th Int. Conf. on Ind. Electron. Contr. and Instrument*, pp. 182-187. Bologna, Italy.

Wung, P. Y. P. and H. B. Puttgen (1992) Synchronous reluctance motor operating point dependent parameter determination. *IEEE Trans Ind. Appl.*, **28**, 358-363.

Xiang, Y. Q. and S. A. Nasar (1995) A fully digital control strategy for synchronous reluctance motor servo drives. *Conf. Rec. IEEE/ IAS Annu. Meet.*, pp. 254-262. Orlando, FL, U.S.A.

Xu, L. X., T. A. Lipo, and D. W Novotny (1991) Vector control of a synchronous reluctance motor including saturation and iron loss. *IEEE Trans. Ind. Appl.*, **27**, 977-985.

同步式磁阻馬達的研究

林明贊　劉添華

國立臺灣工業技術學院電機工程學系

摘　要

本文旨在探討同步式磁阻馬達驅動系統，文中首先建立同步磁阻馬達的數學模式。並說明相關參數的測量方法。其次，在磁場導向控制下提出一個閉迴路驅動系統的簡化模式。在此一簡化模式下，一個滑動模式—模糊控制器被加以設計，經由使用此一新型控制器，整個驅動系統具有快速的響應，以及良好的干擾抗拒能力，然後文中介紹實現整個系統的設計：包含三個軟體程式。32位元C30數位信號處理器系統。與一些簡單的硬體電路。最後，敍述實驗及模擬的結果，實驗的波形與電腦模擬十分吻合，本文提出一磁阻馬達驅動系統的系統化設計方法。